HHS Public Access

Author manuscript

Cell Rep. Author manuscript; available in PMC 2022 July 01.

Published in final edited form as:

Cell Rep. 2022 June 14; 39(11): 110942. doi:10.1016/j.celrep.2022.110942.

Inflammatory adipose activates a nutritional immunity pathway leading to retinal dysfunction

Jacob K. Sterling[1,2], **Bailey Baumann**[1,2], **Sierra Foshe**[1], **Andrew Voigt**[3,4], **Samyuktha Guttha**[1,11], **Ahab Alnemri**[1], **Sam J. McCright**[2,5], **Mingyao Li**[6], **Randy J. Zauhar**[7], **Sandra R. Montezuma**[8], **Rebecca J. Kapphahn**[8], **Venkata R.M. Chavali**[1], **David A. Hill**[5,10], **Deborah A. Ferrington**[8], **Dwight Stambolian**[1], **Robert F. Mullins**[3,4], **David Merrick**[9,10], **Joshua L. Dunaief**[1,12,*]

[1]FM Kirby Center for Molecular Ophthalmology, Scheie Eye Institute, University of Pennsylvania Perelman School of Medicine, Philadelphia, PA 19104, USA

[2]Medical Scientist Training Program, University of Pennsylvania Perelman School of Medicine, Philadelphia, PA 19104, USA

[3]Institute for Vision Research, The University of Iowa, Iowa City, IA 52242, USA

[4]Department of Ophthalmology and Visual Sciences, The University of Iowa Carver College of Medicine, Iowa City, IA 52242, USA

[5]Division of Allergy and Immunology, Children's Hospital of Philadelphia, Philadelphia, PA 19104, USA

[6]Department of Biostatistics, Epidemiology and Informatics, University of Pennsylvania Perelman School of Medicine, Philadelphia, PA 19104, USA

[7]Department of Chemistry & Biochemistry, University of the Sciences, Philadelphia, PA 19104, USA

[8]Department of Ophthalmology and Visual Neurosciences, University of Minnesota, Minneapolis, MN 55455, USA

[9]Department of Medicine, Division of Endocrinology, University of Pennsylvania Perelman School of Medicine, Philadelphia, PA 19104, USA

[*]Correspondence: jdunaief@pennmedicine.upenn.edu.

AUTHOR CONTRIBUTIONS

Conceptualization, J.K.S., B.B., and J.L.D.; investigation, J.K.S., B.B., S.F., A.V., S.G., A.A., S.J.M., and S.R.M.; visualization, J.K.S. and A.V.; funding acquisition, D.S., V.R.M.C., D.M., and J.L.D.; resources, V.R.M.C., D.A.H., D.S., D.A.F., R.J.K., and R.F.M.; supervision, D.S., V.R.M.C., and J.L.D.; writing – original draft, J.K.S. and J.L.D.; writing – review & editing, J.K.S., D.S., D.A.F., V.R.M.C., D.M., and J.L.D.

DECLARATION OF INTERESTS

The authors declare no competing interests.

INCLUSION AND DIVERSITY

One or more of the authors of this paper self-identifies as an underrepresented ethnic minority in science. One or more of the authors of this paper self-identifies as a member of the LGBTQ+ community.

SUPPLEMENTAL INFORMATION

Supplemental information can be found online at https://doi.org/10.1016/j.celrep.2022.110942.

[10]Institute of Diabetes, Obesity and Metabolism, University of Pennsylvania Perelman School of Medicine, Philadelphia, PA 19104, USA

[11]Present address: Department of Ophthalmology, Grossman School of Medicine, New York University, New York, NY 10016, USA

[12]Lead contact

SUMMARY

Age-related macular degeneration (AMD), the leading cause of irreversible blindness among Americans over 50, is characterized by dysfunction and death of retinal pigment epithelial (RPE) cells. The RPE accumulates iron in AMD, and iron overload triggers RPE cell death *in vitro* and *in vivo*. However, the mechanism of RPE iron accumulation in AMD is unknown. We show that high-fat-diet-induced obesity, a risk factor for AMD, drives systemic and local inflammatory circuits upregulating interleukin-1β (IL-1β). IL-1β upregulates RPE iron importers and downregulates iron exporters, causing iron accumulation, oxidative stress, and dysfunction. We term this maladaptive, chronic activation of a nutritional immunity pathway the cellular iron sequestration response (CISR). RNA sequencing (RNA-seq) analysis of choroid and retina from human donors revealed that hallmarks of this pathway are present in AMD microglia and macrophages. Together, these data suggest that inflamed adipose tissue, through the CISR, can lead to RPE pathology in AMD.

In brief

Obesity is a risk factor for age-related macular degeneration (AMD), an ocular disease of the retinal pigment epithelium (RPE). Sterling et al. describe a pathway by which inflammatory adipose triggers iron overload of RPE cells leading to cell dysfunction and oxidative stress. They term this pathway the cellular iron sequestration response (CISR).

Graphical Abstract

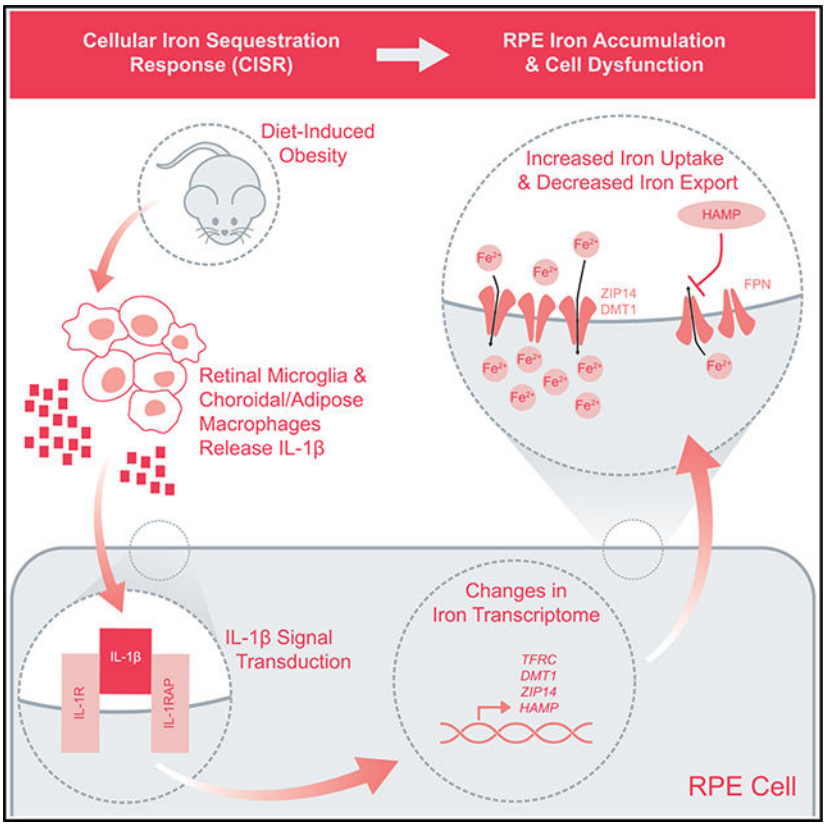

INTRODUCTION

Age-related macular degeneration (AMD) is the leading cause of irreversible blindness in the United States among those 50 years of age and older (Rein et al., 2009). The prevalence of AMD is expected to rise as the US population ages, affecting more than 17 million Americans by 2050 (Rein et al., 2009). Therapies for AMD remain limited. Anti-vascular endothelial growth factor biologics have shown a dramatic ability to slow, but not halt, the progression of neovascular AMD, a subtype of AMD representing only 10% of all cases (Keenan et al., 2020). Unfortunately, there are no therapeutics available to slow progression of non-neovascular AMD, which constitutes ~90% of cases.

The pathophysiology of AMD is characterized by toxic oxidative stress (Beatty et al., 2000; Datta et al., 2017; Age-Related Eye Disease Study 2 Research Group, 2013) and chronic inflammation (Nussenblatt et al., 2014) leading to retinal pigment epithelium (RPE) injury (Hanus et al., 2015) and photoreceptor death. Previous work has shown that iron, a potent cofactor in the formation of reactive oxygen species (ROS) reac (McCord, 1974; McCord and Day, 1978), accumulates in AMD RPE (Hahn et al., 2003).

Since Hahn et al. (2003), multiple studies have linked AMD to iron. Sequence variants in iron-regulatory genes confer genetic risk for AMD (Wysokinski et al., 2011, 2012, 2014, 2015). Exogenous iron supplementation, via intravenous injections of iron sucrose, in wild-type mice and a 43-year-old woman receiving therapy for anemia were associated

with AMD-like retinopathy (Song et al., 2016). *In vitro* and *in vivo* work have established that elevated iron levels upregulate RPE synthesis and secretion of complement component 3 (C3) (Li et al., 2015) and amyloid-β (Guo et al., 2014), two constituents of sub-RPE deposits known as drusen, a key histopathological feature of AMD. Together, these data point to a potential role for iron in the pathogenesis of AMD.

Furthermore, disruption of iron homeostasis in hereditary diseases is sufficient to cause retinal disease in both humans and animal models. Iron overload diseases, including thalassemia (Bhoiwala and Dunaief, 2016) and Friedreich's ataxia (Leruez et al., 2014), can both cause RPE abnormalities. In aceruloplasminemia, loss of ferroxidase ceruloplasmin triggers iron accumulation in the pancreas, brain, and retina, leading to diabetes, dementia, and retinal degeneration (Dunaief et al., 2005). In select cases, patients with aceruloplasminemia exhibit early onset AMD (Dunaief et al., 2005). The analogous mouse model, lacking ceruloplasmin and its homolog, hephaestin (Cp/Heph double knockout [DKO]), exhibits retinal iron accumulation with basal laminar deposits, RPE and photoreceptor degeneration, and subretinal neovascularization (Hahn et al., 2004), all features of AMD. The ocular findings in Cp/Heph DKO animals have been replicated in other animal models of iron accumulation, including Hepc He KO mice (Hadziahmetovic et al., 2011a) and Bmp6 KO mice (Hadziahmetovic et al., 2011b). Together, these data demonstrate that iron accumulation is sufficient for retinal degeneration with features of AMD. Despite abundant data on the link between iron, AMD, and retinal degeneration, the cause of iron accumulation in AMD remains unknown.

High fat intake, also known as a "Western diet," is associated with increased risk of AMD (Chiu et al., 2014; Mares-Perlman et al., 1995; Seddon et al., 2001, 2003a). In mice, high-fat diet potentiates the development of AMD-like features in the retina (Andriessen et al., 2016; Dasari et al., 2011; Espinosa-Heidmann et al.,2006; Fujihara et al.,2009; Jun et al., 2018; Landowski et al., 2019; Roddy et al., 2019; Toomey et al., 2015; Tuzcu et al., 2017; Zhang et al., 2018). As in AMD, mice fed a high-fat diet exhibit increased markers of both systemic and local immune activation in the CNS (Guilherme et al., 2008; Guo et al., 2020; Lumeng and Saltiel, 2011; Vandanmagsar et al., 2011).

Given the independent associations between AMD and a high-fat diet (Chiu et al., 2014; Mares-Perlman et al., 1995; Seddon et al., 2001, 2003a) and AMD and iron accumulation (Hahn et al., 2003), we tested the hypothesis that a high-fat diet induces RPE iron accumulation and oxidative stress. Herein, we show that a high-fat diet leads to the formation of inflammatory adipose tissue, which releases interleukin-1β (IL-1β). IL-1β produced by visceral adipose, and/or locally in ocular tissues, activates the cellular iron sequestration response (CISR), a maladaptive chronic application of nutritional immunity, triggering the deleterious uptake of iron into RPE cells. This in turn leads to RPE oxidative stress and electrophysiological dysfunction. Using human donor tissue, we show that hallmarks of the CISR and IL-1β production pathway are observed in AMD eyes, suggesting that the CISR, identified using the high-fat-diet model, may be active in AMD and contribute to RPE iron accumulation, oxidative stress, and cell death.

RESULTS

High-fat diet induces iron-dependent RPE dysfunction

C57BL/6J wild-type (WT) mice were fed a diet of 10% calories from fat (low-fat diet [LFD]) or 60% calories from fat (high-fat diet [HFD]) alone or in combination with the oral iron chelator deferiprone (DFP) for 12 weeks (from 3 to 6 months of age). DFP has been shown previously to reduce RPE iron levels (Hadziahmetovic et al., 2011c). HFD mice gained weight relative to LFD mice regardless of DFP treatment (Figure 1A). The mass of visceral (visceral adipose tissue [VAT]) and subcutaneous (subcutaneous adipose tissue [SAT]) fat pads was not affected by DFP (Figure 1B). DFP and/or HFD had no effect on glycemic control (Figure 1C) after 12 weeks of treatment, eliminating hyperglycemia as a potential confounding variable in our analyses. We performed inductively coupled plasma mass spectrometry to quantify intracellular iron in RPE isolated from mice in all four groups. HFD mice exhibited increased intracellular RPE iron relative to both LFD groups and HFD mice treated with DFP (Figure 1D). Iron can act as a potent generator of reactive oxygen species (ROS), which can induce oxidative stress, a pathological feature of AMD (Beatty et al., 2000; Brantley et al., 2012; Jun et al., 2018; McCord, 1974; McCord and Day, 1978). To investigate oxidative stress in the RPE, we measured levels of malondialdehyde (MDA), an oxidized lipid product, and *Hmox1* mRNA, which is upregulated by oxidative stress. Levels of both MDA and *Hmox1* mRNA increased in the HFD RPE and were reduced by treatment with DFP (Figures 1E and 1F). To assess RPE function, we performed RPE electrophysiology *in vivo* using electroretinography. In response to light pulses, the RPE exhibits a slow electrical polarization (c wave) whose amplitude can be quantified as a marker of RPE cell health (Wu et al., 2004). The RPE in HFD mice exhibited a c-wave amplitude deficit that was rescued by iron chelation (Figure 1G). Together, these data demonstrate that HFD induces RPE iron accumulation, oxidative stress, and electrical dysfunction, which can be partially rescued by iron-chelation therapy.

IL-1β is necessary for HFD-induced RPE iron accumulation and dysfunction

Although iron accumulation contributes to HFD-induced RPE dysfunction, the cause of iron accumulation in the HFD mouse is not known. Previous work has shown that pro-inflammatory cytokine IL-1β can affect iron homeostasis (Kanamori et al., 2017; Shanmugam et al., 2015; Silva et al., 2019) and is produced by inflamed adipose tissue (Vandanmagsar et al., 2011). We hypothesized that IL-1β triggers RPE iron accumulation. To test this hypothesis, we treated cultured fetal human RPE (fRPE) cells with media or recombinant IL-1β (rIL-1β) in the presence of transferrin-bound radioactive ferric iron ($Tf\cdot{}^{55}Fe^{3+}$) or labile radioactive ferrous iron ($^{55}Fe^{2+}$), the two physiologic forms of extracellular iron. rIL-1β induced ferrous, but not ferric, iron accumulation (Figure 2A). This was accompanied by increased expression of three iron importers, *TfRC*, *DMT1*, and *ZIP14* (Figure 2B). TfRC participates in transferrin-bound ferric-iron import (Daher and Karim, 2017), while both DMT1 (Lane et al., 2010) and ZIP14 (Liuzzi et al., 2006) have been linked to ferrous-iron uptake. Given IL-1β′s ability to trigger RPE iron accumulation *in vitro,* and a pre-existing literature on IL-1β upregulation in inflammatory fat (Vandanmagsar et al., 2011), we hypothesized that IL-1β is necessary for RPE iron accumulation in the HFD mouse. To test this, we fed WT and *Il1b*$^{-/-}$ (KO) mice either an

LFD or an HFD for 12 weeks as described above. Genotype had no effect on total mass gained across the treatment period (Figure 2C) or on the distribution of fat across different fat pads (Figure 2D). Genotype and/or diet also had no effect on glycemic control (Figure 2E). HFD-fed mice exhibited IL-1β-dependent upregulation of *Tfrc*, *Dmt1*, and *Zip14* in RPE, consistent with the gene-expression changes observed in rIL-1β-treated fRPE cells. In addition to upregulation of these three iron importers, RPE from HFD mice also exhibited an IL-1β-dependent upregulation of *Hamp*, which encodes the peptide hormone hepcidin. Hepcidin negatively regulates iron export from the only known mammalian iron exporter, ferroportin (*Fpn*) (Figure 2F). RPE was not the only source of retinal hepcidin production. $CD11b^+$ cells isolated from retina also upregulated *Hamp* in the HFD-fed mice in an IL-1β-dependent manner (Figure 2G). HFD-induced RPE iron accumulation (Figure 2H), MDA elevation (Figure 2I), and *Hmox1* upregulation (Figure 2J) were all IL-1β dependent, as were the c-wave deficits observed in mice fed an HFD (Figure 2J). Together, these data suggest that obesity-associated IL-1β, via upregulation of iron importers and hepcidin, induces RPE iron sequestration, oxidative stress, and dysfunction.

Activation of systemic and local inflammatory circuits contributes to IL-1β production

Given the critical role of IL-1β in RPE iron accumulation, we sought to identify sources of obesity-associated IL-1β, which could contribute to RPE iron accumulation. The RPE itself is sandwiched between the neurosensory retina, located inside the blood-retina barrier, and the choriocapillaris, a highly vascular tissue that bathes the basolateral aspect of the RPE in plasma via fenestrated capillaries (Figure 3A). We measured IL-1β protein levels in a well-characterized subtype of VAT, epididymal white adipose tissue (eWAT), retina, choroid, and serum. IL-1β protein levels were elevated in each tissue in HFD mice (Figure 3B), suggesting that multiple sources of IL-1β could contribute to RPE CISR.

Previous data have shown that both mature adipocytes and adipose tissue resident macrophages produce IL-1β following HFD and formation of inflammatory adipose tissue (Chawla et al., 2011). Given local elevations in IL-1β in the choroid and retina, we wanted to identify candidate cell types that could be responsible for local IL-1β production. IL-1β is produced as a 35 kDa precursor (pro-IL-1β). Following NLRP3 inflammasome activation, it is cleaved by the protease caspase-1 into a 17 kDa active form (IL-1β)(Weber et al., 2010). Based on previous data implicating retinal $CD11b^+$ cells in the production of retinal IL-1β (Natoli et al., 2017), we hypothesized that $CD11b^+$ cells in the retina and choroid contribute to IL-1β production in the HFD model. Unfortunately, *in vivo* measurements of cell-type-specific IL-1β secretion are extremely challenging. To determine if $CD11b^+$ cells in the HFD model are capable of IL-1β production, we defined a state of IL-1β production competence based on expression of *Il1b*, *Nlrp3*, and *Casp1*. $CD11b^+$ cells from retina (Figure 3C) and choroid (Figure 3D) exhibited co-expression of *Il1b*, *Nlrp3*, and *Casp1*. In $CD11b^+$ cells from both sources, *Il1b* mRNA levels were upregulated in the HFD mice (Figures 3C and 3D). Together, these data demonstrate that $CD11b^+$ cells in the retina and choroid are competent to produce IL-1β.

To dissect the contribution of adipose-tissue-derived IL-1β to obesity-associated RPE iron accumulation, $Il1b^{-/-}$ mice on an HFD for 1.5 months were given an eWAT transplant from

Il1b$^{-/-}$ or *Il1b*$^{+/+}$ donor mice. Following transplant, mice were maintained on an HFD for another 1.5 months before they were euthanized (Figure 3E). IL-1β protein levels were measured in serum, choroid, and neurosensory retina using IL-1β ELISA and compared with *Il1b*$^{+/+}$ mice maintained on LFD or HFD for 3 months with a sham transplant surgery at 1.5 months. IL-1β protein levels in the serum were elevated in *Il1b*$^{-/-}$ HFD mice that received transplant tissue from HFD *Il1b*$^{+/+}$ but not HFD *Il1b*$^{-/-}$ mice, suggesting that serum IL-1β is at least partially derived from adipose tissue (Figure 3F). Likewise, choroidal IL-1β protein levels were elevated in *Il1b*$^{-/-}$ mice that received transplant tissue from WT but not *Il1b*$^{-/-}$ mice (Figure 3G). Retina IL-1β levels were low, but not undetectable, following WT adipose transplant (Figure 3H). This may represent contamination from the serum/choroid or transport of IL-1β into the retina across the blood-retina barrier. These data demonstrate that adipose-derived IL-1β contributes to serum and choroidal IL-1β levels.

Finally, we measured RPE iron accumulation in each of the four groups and found that *Il1b*$^{+/+}$ eWAT transplant into *Il1b*$^{-/-}$ mice was sufficient to trigger RPE iron accumulation (Figure 3I). Together, the data in Figures 3F–3I suggest that systemic IL-1β produced by eWAT is sufficient to trigger RPE iron accumulation.

Data from WTLFD-and HFD-fed mice show that IL-1β levels are elevated in multiple compartments including the neurosensory retina (Figure 3B). However, restoration of systemic levels of IL-1β in the serum and choroid, using eWAT transplant, was not sufficient to increase retinal IL-1β levels, suggesting that the elevated IL-1β in retina caused by HFD in WT mice (Figure 3B) results from local production of IL-1β within the retina. To determine if retinal IL-1β is sufficient to induce RPE CISR, adult WT mice were given an intravitreal injection of PBS or rIL-1β (Figure 3J). Inductively coupled plasma mass spectrometry (iCP-MS) performed on RPE isolated 8 hours after injection demonstrated an increase in RPE iron in the rIL-1β-injected eyes compared with the PBS-injected eyes (Figure 3K). These data demonstrate that IL-1β in the retina is also sufficient to induce RPE CISR.

Together, the data in Figures 3B–3K suggest that both systemic and local sources of IL-1β, including inflammatory adipose tissue, choroidal macrophages, and retinal microglia, contribute to RPE CISR in this obese, non-diabetic mouse model.

Hallmarks of IL-1β-dependent CISR are observed in AMD patients

Based on our findings, IL-1β in the systemic circulation, choroid, or neurosensory retina may contribute to RPE iron accumulation (Figure 3). Previous work has shown that IL-1β protein levels are elevated in serum from AMD patients (Nassar et al., 2015), suggesting that systemic IL-1β production may trigger RPE CISR in AMD. Our data also implicate CD11b^{+} cells in the choroid and retina in local IL-1β production. To determine which cell populations are competent to produce IL-1β in humans, we used single-cell RNA sequencing (scRNA-seq) to identify cells that express *IL1B*, *NLRP3*, and *CASP1*. Choroidal scRNA-seq data from human donors (4 with no ocular disease, 2 with AMD) showed that 58.6% of choroidal macrophages were *Il1b+ Nlrp3+ Casp1+* mRNA triple positive (Figure 4A). This expression pattern was specific to macrophages (Figure 4B). Comparing the expression of these three RNAs in AMD versus control choroidal macrophages

demonstrated significant *IL1B* mRNA enrichment in macrophages isolated from AMD cases (Figure 4C).

scRNA-seq performed on neurosensory retina from healthy human donors demonstrated significant enrichment for *IL1B*, *NLRP3*, and *CASP1* transcripts in microglia compared with other retinal cell types (Figure 4D), consistent with our observation that $CD11b^+$ cells in the HFD mouse retina upregulated *Il1b* (Figure 3C). Using the same dataset, we also show that *HAMP*, a negative regulator of iron export, is expressed specifically in retinal microglia (Figure 4E). This is in line with our data showing that retinal $CD11b^+$ cells (enriched for microglia) upregulate *Hamp* in HFD-fed mice (Figure 2G) and recent work that showed that *HAMP* transcripts are enriched in AMD microglia from early AMD MGS2 (Minnesota Grading System [MGS] 2) retinas compared with normal (MGS1) retinas (Lyu et al., 2021). Together, these data support the hypothesis that microglia-produced hepcidin may contribute to RPE CISR.

Bulk neurosensory retina RNA-seq from control, early AMD, and late AMD donors demonstrated enrichment for *IL1B*, *NLRP3*, and *CASP1* transcripts correlated with disease progression in samples from macular retina (MR) (Figure 4F).

While scRNA-seq may be sufficient to determine which cell types are competent to produce IL-1β, ultimately, mature IL-1β must be produced to elicit the RPE CISR. We compared IL-1β protein levels in neurosensory retina (NSR) samples from MGS1 (no AMD) versus MGS2 (early AMD) and MGS3 (intermediate AMD) eyes (see Table S1 for donor information). IL-1β protein levels were significantly elevated in MGS2/3 retinas compared with MGS1 retinas (Figure 4G).

DISCUSSION

We show that HFD-induced obesity leads to upregulation of IL-1β, which triggers RPE iron accumulation, oxidative stress, and electrophysiologic dysfunction. We term this IL-1β-dependent RPE iron accumulation the cellular iron sequestration response (CISR). Both systemic/choroidal and retinal IL-1β were sufficient to induce CISR. Using the HFD mouse model and RNA-seq data from human donors, we implicate choroidal macrophages and retinal microglia in the IL-1β production necessary for RPE CISR. Together, these data demonstrate a pathway of inflammation-driven iron accumulation in a mouse model with links to AMD.

Inflammation is a key regulator of iron homeostasis beyond the CISR mechanism proposed herein. Transition metals, including iron, are essential for prokaryotic and eukaryotic life. To defend against pathogens, vertebrate immune systems can sequester iron as a bacteriostatic mechanism of host defense termed “nutritional immunity” (Lopez and Skaar, 2018; Soares and Weiss, 2015). Anemia of inflammation (AI), a common clinical condition associated with acute (critical illness, infection) and chronic (cancer/hematological malignancies, immune-mediated disease, inflammatory disease, obesity) inflammation is a maladaptive sequela of nutritional immunity. In AI, activation of the innate immune system drives iron sequestration in macrophages via upregulation of cellular iron import and downregulation of

iron export (Soares and Hamza, 2016; Weiss et al., 2019), reminiscent of the same pathways we have described in the retina and involving the same regulators (IL-1β) and effectors (hepcidin).

AMD is associated with elevated serum measures of inflammation, including C-reactive protein, tumor necrosis factor alpha (TNF-α), IL-6, and IL-1β (Haas et al., 2015; Klein et al., 2014; Nassar et al., 2015). Genetic risk factors associated with AMD, including single-nucleotide polymorphisms in both complement factor H and matrix metalloproteinases, are associated with higher serum levels of IL-1β (Budiene et al., 2018; Cao et al., 2013). In humans and mice, visceral adiposity and obesity are associated with systemic inflammation, including elevated levels of serum IL-1β (Chawla et al., 2011; Wu and Ballantyne, 2020). These data, in combination with our own, suggest that systemic inflammation, driven by visceral adiposity, may influence the development and progression of AMD.

Previous work has demonstrated an association between dietary fat, visceral adiposity, and progression of AMD (Adams et al., 2011; Haas et al., 2015; Seddon et al., 2001, 2003b). The link between HFD and AMD has also been borne out in mouse models. HFD in combination with smoke exposure or ingestion of a smoke-related redox molecule, HQ, produced a mouse with sub-RPE deposits, thickening of Bruch's membrane (BM), and deposits within BM–all features of AMD (Espinosa-Heidmann et al., 2006). Sub-RPE deposits, complement activation, RPE damage, and visual function impairment are observed in aged mice carrying genetic risk associated with AMD and fed an HFD (Toomey et al., 2015). In each of these models, HFD, in combination with other factors associated with AMD, induces AMD-like phenotypes in mice. In our obese, non-diabetic mice, we did not observe photoreceptor/RPE cell death or changes in RPE morphology. Based on these data, it seems likely that individual risk factors alone are not sufficient for AMD (Espinosa-Heidmann et al., 2006; Toomey et al., 2015; Zhang et al., 2018), reinforcing a multi-hit hypothesis of AMD pathogenesis (Fritsche et al., 2014).

Inflammasome activation and IL-1β signaling have been observed in the AMD retina (Ambati et al., 2013; Tarallo et al., 2012; Zhao et al., 2015). The RPE of patients with either form of advanced AMD (geographic atrophy and choroidal neovascularization) exhibit elevated levels of NLRP3 inflammasome components, NLRP3 inflammasome activation markers (caspase-1), and IL-1β mRNA (Ambati et al., 2013; Oh et al., 1999; Tarallo et al., 2012; Tseng et al., 2013; Zhao et al., 2015). Pro-IL-1β and mature IL-1β levels are increased in the vitreous of patients with neovascular AMD (Zhao et al., 2015). Mature IL-1β protein levels are elevated in the serum of obese patients (Chawla et al., 2011; Wu and Ballantyne, 2020) and patients with AMD (Nassar et al., 2015).

Genetic risk factors associated with AMD, including single-nucleotide polymorphisms in both complement factor H and matrix metalloproteinases, are associated with elevated serum levels of IL-1β (Budiene et al., 2018; Cao et al., 2013). In patients with geographic atrophy, sites of cone outer-segment atrophy are associated with macrophages in retinal tissue sections. *In vivo*, macrophages in the retina express elevated levels of IL-1β, suggesting that IL-1β may play a role in cone outer-segment atrophy and disease progression (Doyle et al., 2014). IL-1β treatment of RPE leads to cell swelling and atrophy *in vivo* (Doyle et al.,

2014). Components of drusen, including Aβ (1–40), increase the expression of IL-1β and inflammasome components *in vivo* (Celkova et al., 2015). Together, these data suggest that IL-1β may contribute to AMD pathogenesis.

Herein, we implicate $CD11b^+$ cells of the retina and choroid in the production of IL-1β that triggers RPE CISR, based on expression of *Il1b*, *Nlrp3*, and *Casp1* mRNA. We define triple-positive cells as "competent for IL-1β production." However, release of IL-1β is itself a regulated step in the inflammatory cascade that can occur via gasdermin-dependent and -independent pathways (Monteleone et al., 2018). Our data showing that eWAT transplantation from HFD/$Il1b^{+/+}$ into HFD/$Il1b^{-/-}$ mice can induce RPE CISR also suggests that systemic IL-1β can induce RPE CISR. Future work is necessary to understand the molecular signals that lead to microglial and choroidal macrophage IL-1β production and secretion in the high HFD and AMD.

Of note, $CD11b^+$ cells may not be the only sources of IL-1β in the AMD retina. Previous work has documented increased NLRP3 inflammasome components and *IL1B* mRNA in the RPE of patients with either form of advanced AMD (geographic atrophy or choroidal neovascularization) (Celkova et al., 2015; Oh et al., 1999; Tseng et al., 2013; Zhao et al., 2015). Although the RPE of the HFD mice did not upregulate *Il1b*, *Nlrp3*, or *Casp1* (data not shown), AMD RPE may serve as a source of IL-1β. This IL-1β could act in an autocrine fashion, triggering RPE CISR. Since iron itself can activate the RPE inflammasome (Gelfand et al., 2015), autocrine RPE IL-1β signaling could trigger a vicious cycle of iron and inflammation leading to RPE degeneration.

The data herein spur a number of avenues for future exploration. Future work should determine whether the CISR is reversible and whether change in diet can reduce RPE iron accumulation, oxidative stress, and dysfunction. Additionally, we chose to focus our work on the RPE; however, CISR may occur in other cells types, including the photoreceptors, which have previously been shown to exhibit iron accumulation in AMD (Dentchev et al., 2005). CISR in microglia may also lead to further inflammation based on previous work showing that iron accumulation leads to microglial production of cytokines (Nnah et al., 2020). Finally, prospective studies should assess the role of systemic inflammation in obesity as a determinant of AMD risk. Beyond the context of AMD, other CNS diseases exhibit co-incident iron accumulation, neuroinflammation, and degeneration, including Parkinson's disease (Jiang et al., 2016; Wood, 2020; Sterling et al., 2022) and Alzheimer's disease (Connor et al., 1992). It is therefore possible that the CISR mechanism described herein may be relevant to those neurodegenerative diseases as well as chronic systemic inflammatory diseases.

Iron accumulation in AMD RPE was first described in 2003. Since then, multiple publications have demonstrated that iron accumulation is sufficient for retinal degeneration with features of AMD, including RPE oxidative stress, dysfunction, and retinal degeneration with neovascularization. However, the potential use of iron chelator DFP in AMD has been hampered by its side effects, including rare, but potentially deadly, neutropenia and agranulocytosis, which require weekly monitoring. Our findings provide an AMD-linked mechanism for RPE iron accumulation, oxidative stress, and RPE dysfunction, which

we term the CISR. Activation of the CISR, via IL-1β, may contribute to RPE iron accumulation in AMD. By identifying IL-1β as a potential causative factor, we open additional translational avenues to reduce iron accumulation in the AMD retina, including intravitreal or systemic administration of FDA-approved anti-IL-1β therapies.

Limitations of the study

Of note, the HFD model of diet-induced obesity is not a one-to-one correlate to HFD/obesity-associated increases in AMD risk. In the HFD model, mice consume significantly more calories than their control-fed counterparts on day 1. Over the ensuing week, their caloric intake normalizes to the level seen in control mice as they consume less food (measured by grams consumed per day) (Benani et al., 2012). Therefore, HFD mice examined at the 3 month time point used herein are obese due to consumption of HFD, not increased calories per day. This contrasts with humans where the effects of HFD, obesity, and increased caloric intake are more challenging to dissect in observational studies examining diet and risk of AMD. Based on the data presented herein, we would hypothesize that inflammatory adipose tissue drives some component of AMD risk associated with HFD.

In this study, we report HFD-induced upregulation of IL-1β across several tissues, measured by ELISA. A caveat to this assay is its inability to distinguish pro-IL-1β from mature, active IL-1β. However, *Il1b* KO abolished the CISR, which was reversed by transplantation of *Il1b*+/+ eWAT. These data suggest that functional IL-1β is necessary to activate the CISR in our HFD model. We therefore conclude that the increase in IL-1β detected by ELISA is most likely due, at least in part, to an increase in the active form.

The data herein do not address the mechanism triggering IL-1β production. In adipose tissue, cross talk between macrophages and mature adipocytes via CCL2, OPN, and saturated fatty acids triggers local inflammation, additional monocyte recruitment into the tissue, and production of proinflammatory cytokines including IL-1β (Chawla et al., 2011; Vandanmagsar et al., 2011). It is not known which of these known, or perhaps an unknown, factors triggers upregulation of *Il1b*, *Nlrp3*, and *Casp1* in retinal microglial cells in our model. However, previous work has shown that in the brain, deletion of microglial IL-1R1 reduces neuroinflammation in the HFD model (Guo et al., 2020). Based on these data, we hypothesize that systemic IL-1β secreted by tissue adipose macrophages may trigger retinal microglial IL-1β production.

STAR*METHODS

RESOURCE AVAILABILITY

Lead contact—Further information and requests for resources and reagents should be directed to and will be fulfilled by the lead contact, Joshua Dunaief (jdunaief@pennmedicine.upenn.edu).

Materials availability—This study did not generate new unique reagents.

Data and code availability—Single-cell and bulk RNA-seq data have been deposited at GEO and are publicly available as of the date of publication. Accession numbers are listed in the key resources table.

This paper does not report original code.

Any additional information required to reanalyze the data reported in this paper is available from the lead contact upon request.

EXPERIMENTAL MODEL AND SUBJECT DETAILS

Animals—For all experiments, mice were housed in a ventilated rack with ad libitum access to food and water under a 12hr light/dark schedule (lights-on at 6:00AM). 12-week-old (wo) male C57BL6/J WT (Jackson Laboratory, 000664) and IL-1β KO mice (Horai et al., 1998), generously provided by Dr. Iwakura, University of Tokyo, were bred in-house for these experiments. Mice were fed either a low-fat diet (Research Diets, D12450) or high fat diet (Research Diets, D12492) starting at 12 wo until 24 wo. Where indicated, mice were treated with 0.5 mg/mL deferiprone (ApoPharma, Toronto, Canada) dissolved in their drinking water starting at 12 wo and continuing until euthanasia. Previous data have shown that this dose is sufficient to reduce iron-induced neurodegeneration in mice (Hadziahmetovic et al., 2011c, 2012; Song et al., 2012). All housing, breeding, and procedures were performed according to the NIH Guide for the Care and Use of Experimental Animals, ARVO standards for the use of animals and approved by the University of Pennsylvania Animal Care and Use Committee.

Primary cell cultures – Fetal retinal pigment epithelium—Highly polarized primary RPE monolayers were established using donor fetal eyes (Advanced Bioscience Resources Inc., Alameda, CA) as previously described (Lyssenko et al., 2018). Each eye was placed in an antibiotic-antimycotic solution and rinsed with Hank's buffered salt solution. The eyes were pinned onto a dissection stage, and the cornea, vitreous, and lens were removed. The open eyes were transferred into a well of a 6 well plate containing room temperature dispase solution in RPE medium/5% FBS and incubated for 45 min at 37°C in 5% CO2. The RPE medium was prepared as previously described (Lyssenko et al., 2018). The retina was removed, and the RPE was peeled off the choroid-scleral tissue. The RPE layer was collected into a 15 mL conical tube, gently shaken, and trypsinized to release RPE cells. The cells were centrifuged, washed, transferred to a T-25 flask, and cultured in RPE medium/15% FBS for 1 week and then in RPE medium/5% FBS for 1 month. By this time, the RPE cells were highly pigmented and confluent at about 500,000 cells/cm2. The cells were transferred onto 0.4 mm pore size polycarbonate 12-well plate inserts (Corning, NY, USA) that were coated with human extracellular matrix, cultured for 5 weeks in RPE medium/15% FBS and then maintained in RPE medium/2% FBS. The barrier function of the RPE monolayer was assessed by measuring transepithelial electrical resistance (TEER), and all had above 450 mΩ.

METHOD DETAILS

Inductively coupled plasma mass spectrometry—Samples were analyzed for metals using a Nexion 300D (PerkinElmer, Shelton, CT). The analytical standards were purchased from SCP (Champlain, NY) and trace metal grade nitric acid was purchased from Fisher Scientific (Pittsburgh, PA). All dilutions will be done using in-house deionized water (≥18 MΩ) obtained from a water purification system (EMD Millipore, Billerica, MA). The dried bovine liver sample (1577 C) used as reference material was obtained from NIST (National Institute of Standards and Technology, Gaithersburg, MD). The tissue samples were dried overnight in an oven set at 70°C and then weighed into Teflon PFA vials (Savillex, Minnetonka, MN). The dried tissue samples were then digested overnight with 20 times the quantity (weight/volume) of 70% nitric acid at 70°C. A 0.1 mL portion of the digested tissue sample was then mixed with 0.05 mL of 2 ppm internal standard containing Ge (germanium), In (indium), Tb (terbium), and Y (yttrium) and the mixture was diluted with deionized water to a final volume of 5 mL for analysis. The concentration of each metal in the submitted sample was measured using a calibration curve of aqueous standards prepared at four different concentrations of each metal. The accuracy of the results was monitored by analyzing reference material (NIST 1577C) with known values of metals of interest with each batch of samples. Total iron measurements for each sample were normalized to the number of cells in the sample.

MDA ELISA—MDA competitive ELISA kit from Abcam (ab238537) was used accounting to manufacturer's protocol. Briefly, isolated RPE cells were lysed, and cell lysates were placed in an MDA conjugate coated plate. After incubation the wells of the plate were labeled with an HRP-conjugate secondary antibody. Absorbance at 450nm was quantified and compared to a standard curve to quantify the amount of MDA present in the experimental samples. All measurements shown herein are the average of two technical replicates.

Quantitative PCR—RNA isolation was performed according to the manufacturer's protocol (RNeasy kit; Qiagen). cDNA was synthesized with reverse transcription agents (TaqMan Reverse Transcription Reagents, Applied Biosystems) according to the manufacturer's protocol. Gene expression was analyzed using a commercial sequence detection system (ABI Prism 7500, Applied Biosystems). All reactions were performed in technical triplicate. Probes were obtained from ThermoFisher Scientific.

Electroretinography—Mice were dark-adapted overnight, anesthetized with a ketamine-xylazine cocktail delivered intramuscularly, their pupils were dilated with 1% tropicamide (Alcon Laboratories, Fort Worth, TX), and the animals were placed on a stage maintained at 37°C. Custom made clear plastic contact lenses with embedded platinum wires served as recording electrodes, and a platinum wire loop inserted into the animal's mouth served as the reference electrode. Electroretinograms were elicited and recorded with an Espion E3 apparatus (Diagnosys LLC, Lowell, MA). C-wave responses were obtained with stimuli of 0.1, 1, 10 and 100 scot cd s m^{-2} delivered at 10 s intervals. Values and representative recordings reported herein were recorded at 100 scot cd s m^{-2}.

Fetal RPE cell culture treatment & gene expression studies—For IL-1β treatment cells were placed in serum free media for 24 h prior to start of experiment. After 24 h, the fRPE cells were treated with vehicle or 10 ng/mL IL-1β (Abcam, Ab9617) for 24 h before harvest.

Fetal RPE cell culture radiolabeled ^{55}Fe tracing studies—To directly measure intracellular iron accumulation in response to IL-1β treatment, radiolabeled ^{55}Fe tracking studies were completed in IL-1β-treated fRPE cells. fRPE cells were grown on 12 well transwell plates (Corning, Corning, NY, USA). 24 h before the start of the experiment, the cells were placed into serum-free media. After 24 h, the cells were given either vehicle or 10 ng/mL IL-1β. After 24 h of IL-1β treatment, iron uptake was assessed with 2 μM 55Fe in two forms, as holo-Tf (Sigma-Aldrich, St. Louis, MO, USA) (Tf-$^{55}Fe^{3+}$) or as $^{55}Fe^{2+}$ ascorbate. The radiolabeled holo-transferrin was prepared by adding 100 μM 55Fe2+Cl3 to 100 μM apo-transferrin made up in loading buffer consisting of 1 M Hepes KOH pH 7.5, 150 mM NaCl, 10 mM freshly prepared sodium bicarbonate, incubating for 30 min on ice and rapidly centrifuging through a G25 column. This stock was diluted 1:50 into serum free medium to give a concentration of 2 μM iron for the assay. The $^{55}Fe^{2+}$ ascorbate was prepared by adding 1 mM sodium ascorbate (Sigma-Aldrich, St. Louis, MO, USA) to 100 μM $55Fe^{2+}Cl_3$ in a small volume, incubating 10 min in air, and then diluting 1:50 into serum free medium to give a concentration of 2 μM iron for the assay. Iron uptake was allowed to proceed for 6 h. After 6 h, cell lysates were collected in 1X RIPA buffer (Cell Signaling Technology, Danvers, MA, USA). 100ul of the cell lysate was added to a scintillation tube with 1mL of scintillation liquid (Catalog #: SX20-5, Fisher Scientific, Pittsburgh, PA, USA). The iron counts per minute (CPM) in the lysates were then measured in a scintillation counter.

Magnetic activated cell sorting for CD11b+ cells—All cell sorting steps relied on Miltenyi Biotec Microbead Kits: Anti-ACSA-2 Microbead (Cat # 130-097-678), Anti-CD11b Microbead (Cat # 130-126-725). Briefly, at each selection step Fc receptors were blocked with an FcR Blocking Reagent. Cells were then incubated with a magnetically labeled antibody targeting the epitope of interest (ACSA-2, CD11b). The cell suspension was passed through an MS column (Miltenyi Biotec, Cat # 130-042-201) in a magnetic field so that magnetically labeled cells remained in the column while unlabeled cells passed through the column. This process was repeated twice over two separate MS columns to maximize purity of the isolated population. Retinal CD11b+ cells were isolated by a two-step process: first selecting against ACSA2 and then selecting for CD11b as described previously (Sterling et al., 2020). Choroidal CD11b+ cells were isolated using a single positive selection step for CD11b.

IL-1β ELISA—Human and mouse IL-1β was measured in protein lysates and serum using kits from R&D Systems (MLB00C or DLB50 R&D Systems) following the manufacturer's instructions. All mice were perfused prior to tissue harvest for all ELISA measurements on adipose tissue, retina, and choroid.

Epididymal white adipose tissue transplant—Donors (both *Il1b+/+* or *Il1b−/−* mice) and recipients (*Il1b−/−* mice) were maintained on a high fat diet for 6 weeks. At 6 weeks epididymal white adipose tissue (EWAT) was harvested from donor mice (*Il1b+/+* or *Il1b−/−*) and transplanted into recipient mice. Briefly, an aseptic surgical area was prepared, and mice were anesthetized using isoflurane. Following anesthesia, an abdominal skin and peritoneal incision was made to expose the viscera. Donor EWAT was exposed, and a scalpel was used to expose the EWAT vasculature in the recipient. Donor EWAT tissue was sutured into the host EWAT, proximal to the exposed vasculature. The peritoneal cavity and skin were closed, and the mouse was fully alert before being returned to the animal colony. Mice were provided with post-surgical antibiotics and analgesia. Recipient mice were maintained on a high fat diet for another 6 weeks before euthanasia. Transplant tissue was assessed following euthanasia by gross examination to determine if the donor tissue (marked by a non-absorbable suture) was well vascularized. Mice in which the suture could not be located or where the tissue surrounding the suture appeared poorly vascularized or necrotic were excluded from the study.

Intravitreal injection—2 μg/mL recombinant murine IL-1β (Pharmingen, San Diego, CA, USA), diluted in 1XPBS, was injected into the vitreous of the right eyes of C57BL/6J male mice, resulting in 2 ng of IL-1β protein total delivered to the vitreous. The left eyes received intravitreal injections of vehicle, using a 10- μL syringe (Hamilton, Martinsried, Germany) fitted with a 35-gauge needle. 2ng of IL-1β was chosen because in the 4.4μL volume of the mouse vitreous, the concentration of IL-1β was the same order of magnitude as the concentration of IL-1β observed in neovascular AMD and polypoidal choroidal vasculopathy (Zhao et al., 2015). After 8 h the mice were euthanized, and eyes were processed for analysis.

Choroid single-cell RNAseq—Previously published human choroidal single-cell RNA sequencing data were reprocessed from four adult control donors and two adult AMD donors (GSE135922 donors 4–7, GSE149100 donors 22–23) (Voigt et al., 2019; 2020a) using the Seurat R package (Butler et al., 2018). Using this data, we investigated which cell type(s) expressed *IL1B, NLRP3,* and *CASP1.* All cells that expressed at least one read of *IL1B, NLRP3,* and *CASP1* were classified as ‘triple-positive’ cells for visualizations. Differential expression analysis was performed between the macrophage cells from AMD versus control donors using the FindMarkers function (using the Wilcoxon Rank Sum test) within Seurat. Visualizations of single-cell RNA sequencing data were created with Spectacle (Voigt et al., 2020b), which also allows for online interactive analysis of this dataset.

Neurosensory retina single-cell RNAseq—The scRNA-seq data were generated from macular and peripheral retina taken from two healthy adult donors using the 10X Genomics Chromium system. Neither donor had a known history of retinal disease, head or ocular trauma, significant refractive error, neurological disease, diabetes, or uncontrolled hypertension. Cell types in the retina that expressed *IL1B*, *NLRP3*, or *CASP1* in at least 10% of their cells were classified as positively expressing the gene. Expression output was

mapped to the tSNE coordinates in R to produce the landscape plots. Additional information can be found in the original publication documenting these results (Lyu et al., 2021).

Neurosensory retina Bulk-RNAseq—The bulk RNA-data were generated from 13 macula samples (6 normal, 4 early AMD, and 3 late AMD) and 15 periphery samples (8 normal, 4 early AMD, and 3 late AMD) taken from the retina of 15 adult donors. RNA for the eye tissues was extracted using the AllPrep DNA/RNA Mini Kit (Qiagen). RNA sequencing was performed at the Center for Applied Genomics at the Children's Hospital of Philadelphia per standard protocols. The prepared libraries were clustered and then sequenced using HiSeq 2000 sequencer (Illumina, Inc., San Diego, CA, USA) with four RNA-seq libraries per lane (2 × 101-bp paired-end reads). The RNA-Seq data were aligned to the hg38 reference genome using GSNAP (version 2016-06-30). The expression of all genes annotated in the hg38 assembly was quantitated in units of FPKM (fragments per kilobase exon per million mapped reads) using CUFFQUANT (version 2.2.1), and differential expression between Normal samples and AMD samples, including assignment of statistical significance, was assessed for each sample region using CUFFDIFF (version 2.2.1). Additional information can be found in the original publication documenting these results (Lyu et al., 2021). Using this data, we investigated the RNA expression of *IL1B*, *NLRP3*, and *CASP1*.

QUANTIFICATION AND STATISTICAL ANALYSIS

Statistical analyses for each panel are described in figure legends. *N* represents biological replicates. SEM is shown unless otherwise stated. All statistical analyses were performed using GraphPad Prism 9.0 (San Diego, CA, USA).

Supplementary Material

Refer to Web version on PubMed Central for supplementary material.

ACKNOWLEDGMENTS

Funding for J.K.S. was provided by the National Institutes of Health/National Eye Institute (F30EY032339). Funding for J.K.S., B.B., S.F., S.G., A.A., and J.L.D. was provided by the National Institutes of Health/National Eye Institute (R01EY028916), Research to Prevent Blindness, the FM Kirby Foundation, the Paul and Evanina Bell Mackall Foundation Trust, and a gift in memory of Lee F. Mauger, MD. Funding for S.F. was provided by Graduate Training in Neuroscience (T32NS105607). Funding for S.J.M. was provided by the Michael Brown Fellowship. Funding for D.A.H. and S.J.M. was provided by the National Institutes of Health (K08 DK116668). Funding for S.R.M., R.J.K., and D.A.F. was provided by the National Institutes of Health/National Eye Institute (R01EY026012), Elaine and Robert Larson Endowed Vision Research Chair and Helen Lindsay Family Foundation, and the Knobloch Chair Professorship. Funding for V.R.M.C. was provided by the National Institutes of Health/ National Eye Institute (R21EY028273). Funding for M.L. was provided by the National Institutes of Health/National Eye Institute (R01EY030192, R21EY031877, and R01EY031209). Funding for D.S. was provided by the National Institutes of Health/National Eye Institute (R01EY031209). Funding for D.M. was provided by the National Institutes of Health/National Institute of Diabetes and Digestive and Kidney Disease (K08DK122099).

REFERENCES

Adams MKM, Simpson JA, Aung KZ, Makeyeva GA, Giles GG, English DR, Hopper J, Guymer RH, Baird PN, and Robman LD (2011). Abdominal obesity and age-related macular degeneration. Am. J. Epidemiol 173, 1246–1255. 10.1093/aje/kwr005. [PubMed: 21422060]

Age-Related Eye Disease Study 2 Research Group (2013). Lutein + zeaxanthin and omega-3 fatty acids for age-related macular degeneration: the Age-Related Eye Disease Study 2 (AREDS2) randomized clinical trial. JAMA 309, 2005–2015. 10.1001/jama.2013.4997. [PubMed: 23644932]

Ambati J, Atkinson JP, and Gelfand BD (2013). Immunology of age-related macular degeneration. Nat. Rev. Immunol 13, 438–451. 10.1038/nri3459. [PubMed: 23702979]

Andriessen EM, Wilson AM, Mawambo G, Dejda A, Miloudi K, Sennlaub F, and Sapieha P (2016). Gut microbiota influences pathological angiogenesis in obesity-driven choroidal neovascularization. EMBO Mol. Med 8, 1366–1379. 10.15252/emmm.201606531. [PubMed: 27861126]

Beatty S, Koh H, Phil M, Henson D, and Boulton M (2000). The role of oxidative stress in the pathogenesis of age-related macular degeneration. Surv. Ophthalmol 45, 115–134. 10.1016/s0039-6257(00)00140-5. [PubMed: 11033038]

Benani A, Hryhorczuk C, Gouaze A, Fioramonti X, Brenachot X, Guissard C, Krezymon A, Duparc T, Colom A, Nedelec E, et al. (2012). Food intake adaptation to dietary fat involves PSA-dependent rewiring of the arcuate melanocortin system in mice. J. Neurosci 32, 11970–11979. 10.1523/jneurosci.0624-12.2012. [PubMed: 22933782]

Bhoiwala DL, and Dunaief JL (2016). Retinal abnormalities in β-thalassemia major. Surv. Ophthalmol 61, 33–50. 10.1016/j.survophthal.2015.08.005. [PubMed: 26325202]

Brantley MA, Osborn MP, Sanders BJ, Rezaei KA, Lu P, Li C, Milne GL, Cai J, and Sternberg P (2012). Plasma biomarkers of oxidative stress and genetic variants in age-related macular degeneration. Am. J. Ophthalmol 153, 460–467.e1. 10.1016/j.ajo.2011.08.033. [PubMed: 22035603]

Budiene B, Liutkeviciene R, Gustiene O, Ugenskiene R, Laukaitiene D, Savukaityte A, Vilkeviciute A, Steponaviciute R, Rocyte A, and Zaliuniene D (2018). The association of matrix metalloproteinases polymorphisms and interleukins in advanced age-related macular degeneration. Ophthalmic Genet. 39, 463–472. 10.1080/13816810.2018.1484928. [PubMed: 29947568]

Butler A, Hoffman P, Smibert P, Papalexi E, and Satija R (2018). Integrating single-cell transcriptomic data across different conditions, technologies, and species. Nat. Biotechnol 36, 411–420. 10.1038/nbt.4096. [PubMed: 29608179]

Cao S, Ko A, Partanen M, Pakzad-Vaezi K, Merkur AB, Albiani DA, Kirker AW, Wang A, Cui JZ, Forooghian F, and Matsubara JA (2013). Relationship between systemic cytokines and complement factor H Y402H polymorphism in patients with dry age-related macular degeneration. Am. J. Ophthalmol 156, 1176–1183. 10.1016/j.ajo.2013.08.003. [PubMed: 24083687]

Celkova L, Doyle SL, and Campbell M (2015). NLRP3 inflammasome and pathobiology in AMD. J. Clin. Med 4, 172–192. 10.3390/jcm4010172. [PubMed: 26237026]

Chawla A, Nguyen KD, and Goh YPS (2011). Macrophage-mediated inflammation in metabolic disease. Nat. Rev. Immunol 11, 738–749. 10.1038/nri3071. [PubMed: 21984069]

Chiu C-J, Chang M-L, Zhang FF, Li T, Gensler G, Schleicher M, and Taylor A (2014). The relationship of major American dietary patterns to age-related macular degeneration. Am. J. Ophthalmol 158, 118–127.e1. 10.1016/j.ajo.2014.04.016. [PubMed: 24792100]

Connor JR, Menzies SL, St Martin SM, and Mufson EJ (1992). A histochemical study of iron, transferrin, and ferritin in Alzheimer's diseased brains. J. Neurosci. Res 31, 75–83. 10.1002/jnr.490310111. [PubMed: 1613823]

Daher R, and Karim Z (2017). Iron metabolism: state of the art. Transfus. Clin. Biol 24, 115–119. 10.1016/j.tracli.2017.06.015. [PubMed: 28694024]

Dasari B, Prasanthi JR, Marwarha G, Singh BB, and Ghribi O (2011). Cholesterol-enriched diet causes age-related macular degeneration-like pathology in rabbit retina. BMC Ophthalmol. 11, 22. 10.1186/1471-2415-11-22. [PubMed: 21851605]

Datta S, Cano M, Ebrahimi K, Wang L, and Handa JT (2017). The impact of oxidative stress and inflammation on RPE degeneration in non-neovascular AMD. Prog. Retin. Eye Res 60, 201–218. 10.1016/j.preteyeres.2017.03.002. [PubMed: 28336424]

Dentchev T, Hahn P, and Dunaief JL (2005). Strong labeling for iron and the iron-handling proteins ferritin and ferroportin in the photoreceptor layer in age-related macular degeneration. Arch. Ophthalmol 123, 1745. 10.1001/archopht.123.12.1745. [PubMed: 16344450]

Doyle SL, Ozaki E, Brennan K, Humphries MM, Mulfaul K, Keaney J, Kenna PF, Maminishkis A, Kiang A-S, Saunders SP, et al. (2014). IL-18 attenuates experimental choroidal neovascularization as a potential therapy for wet age-related macular degeneration. Sci. Transl. Med 6, 230ra44. 10.1126/scitranslmed.3007616.

Dunaief JL, Richa C, Franks EP, Schultze RL, Aleman TS, Schenck JF, Zimmerman EA, and Brooks DG (2005). Macular degeneration in a patient with aceruloplasminemia, a disease associated with retinal iron overload. Ophthalmology 112, 1062–1065. 10.1016/j.ophtha.2004.12.029. [PubMed: 15882908]

Espinosa-Heidmann DG, Suner IJ, Catanuto P, Hernandez EP, Marin-Castano ME, and Cousins SW (2006). Cigarette smoke–related oxidants and the development of sub-RPE deposits in an experimental animal model of dry AMD. Invest. Ophthalmol. Vis. Sci 47, 729–737. 10.1167/iovs.05-0719. [PubMed: 16431974]

Fritsche LG, Fariss RN, Stambolian D, Abecasis GR, Curcio CA, and Swaroop A (2014). Age-related macular degeneration: genetics and biology coming together. Annu. Rev. Genom. Hum. Genet 15, 151–171. 10.1146/annurev-genom-090413-025610.

Fujihara M, Bartels E, Nielsen LB, and Handa JT (2009). A human apoB100 transgenic mouse expresses human apoB100 in the RPE and develops features of early AMD. Exp. Eye Res 88, 1115–1123. 10.1016/j.exer.2009.01.017. [PubMed: 19450445]

Gelfand BD, Wright CB, Kim Y, Yasuma T, Yasuma R, Li S, Fowler BJ, Bastos-Carvalho A, Kerur N, Uittenbogaard A, et al. (2015). Iron toxicity in the retina requires alu RNA and the NLRP3 inflammasome. Cell Rep. 11, 1686–1693. 10.1016/j.celrep.2015.05.023. [PubMed: 26074074]

Guilherme A, Virbasius JV, Puri V, and Czech MP (2008). Adipocyte dysfunctions linking obesity to insulin resistance and type 2 diabetes. Nat. Rev. Mol. Cell Biol 9, 367–377. 10.1038/nrm2391. [PubMed: 18401346]

Guo LY, Alekseev O, Li Y, Song Y, and Dunaief JL (2014). Iron increases APP translation and amyloid-beta production in the retina. Experimental Eye Research 129, 31–37. 10.1016/j.exer.2014.10.012. [PubMed: 25456519]

Guo D-H, Yamamoto M, Hernandez CM, Khodadadi H, Baban B, and Stranahan AM (2020). Visceral adipose NLRP3 impairs cognition in obesity via IL-1R1 on CX3CR1+ cells. J. Clin. Invest 130, 1961–1976. 10.1172/jci126078. [PubMed: 31935195]

Haas P, Kubista KE, Krugluger W, Huber J, and Binder S (2015). Impact of visceral fat and pro-inflammatory factors on the pathogenesis of age-related macular degeneration. Acta Ophthalmol. 93, 533–538. 10.1111/aos.12670. [PubMed: 25683020]

Hadziahmetovic M, Song Y, Ponnuru P, Iacovelli J, Hunter A, Haddad N, Beard J, Connor JR, Vaulont S, and Dunaief JL (2011a). Age-dependent retinal iron accumulation and degeneration in hepcidin knockout mice. Invest. Ophthalmol. Vis. Sci 52, 109–110. 10.1167/iovs.106113. [PubMed: 20811044]

Hadziahmetovic M, Song Y, Wolkow N, Iacovelli J, Kautz L, Roth MP, and Dunaief JL (2011b). Bmp6 regulates retinal iron homeostasis and has altered expression in age-related macular degeneration. Am. J. Pathol 179, 335–348. 10.1016/j.ajpath.2011.03.033. [PubMed: 21703414]

Hadziahmetovic M, Song Y, Wolkow N, Iacovelli J, Grieco S, Lee J, Lyubarsky A, Pratico D, Connelly J, Spino M, et al. (2011c). The oral iron chelator deferiprone protects against iron overload-induced retinal degeneration. Invest. Ophthalmol. Vis. Sci 52, 959–968. 10.1167/iovs.10-6207. [PubMed: 21051716]

Hadziahmetovic M, Pajic M, Grieco S, Song Y, Song D, Li Y, Cwanger A, Iacovelli J, Chu S, Ying G.s., et al. (2012). The oral iron chelator deferiprone protects against retinal degeneration induced through diverse mechanisms. Transl. Vis. Sci. Technol 1, 2. 10.1167/tvst.1.3.2.

Hahn P, Milam AH, and Dunaief JL (2003). Maculas affected by age-related macular degeneration contain increased chelatable iron in the retinal pigment epithelium and Bruch's membrane. Arch. Ophthalmol 121, 1099. 10.1001/archopht.121.8.1099. [PubMed: 12912686]

Hahn P, Qian Y, Dentchev T, Chen L, Beard J, Harris ZL, and Dunaief JL (2004). Disruption of ceruloplasmin and hephaestin in mice causes retinal iron overload and retinal degeneration with features of age-related macular degeneration. Proc. Natl. Acad. Sci. U S A 101, 13850–13855. 10.1073/pnas.0405146101. [PubMed: 15365174]

Hanus J, Anderson C, and Wang S (2015). RPE necroptosis in response to oxidative stress and in AMD. Ageing Res. Rev 24, 286–298. 10.1016/j.arr.2015.09.002. [PubMed: 26369358]

Horai R, Asano M, Sudo K, Kanuka H, Suzuki M, Nishihara M, Takahashi M, and Iwakura Y (1998). Production of mice deficient in genes for interleukin (IL)-1α, IL-1β, IL-1α/β, and IL-1 receptor antagonist shows that IL-1β is crucial in turpentine-induced fever development and glucocorticoid secretion. J. Exp. Med 187, 1463–1475. 10.1084/jem.187.9.1463. [PubMed: 9565638]

Jiang H, Wang J, Rogers J, and Xie J (2016). Brain iron metabolism dysfunction in Parkinson's disease. Mol. Neurobiol 54, 3078–3101. 10.1007/s12035-016-9879-1. [PubMed: 27039308]

Jun S, Datta S, Wang L, Pegany R, Cano M, and Handa JT (2018). The impact of lipids, lipid oxidation, and inflammation on AMD, and the potential role of miRNAs on lipid metabolism in the RPE. Exp. Eye Res 181, 346–355. 10.1016/j.exer.2018.09.023. [PubMed: 30292489]

Kanamori Y, Murakami M, Sugiyama M, Hashimoto O, Matsui T, and Funaba M (2017). Interleukin-1β (IL-1β) transcriptionally activates hepcidin by inducing CCAAT enhancer-binding protein δ (C/EBPδ) expression in hepatocytes. J. Biol. Chem 292, 10275–10287. 10.1074/jbc.m116.770974. [PubMed: 28438835]

Keenan TD, Vitale S, Agrón E, Domalpally A, Antoszyk AN, Elman MJ, Clemons TE, Chew EY, and Age-Related Eye Disease Study 2 Research Group. (2020). Visual acuity outcomes after anti–vascular endothelial growth factor treatment for neovascular age-related macular degeneration. Ophthalmol. Retin 4, 3–12. 10.1016/j.oret.2019.06.001.

Klein R, Myers CE, Cruickshanks KJ, Gangnon RE, Danforth LG, Sivakumaran TA, Iyengar SK, Tsai MY, and Klein BEK (2014). Markers of inflammation, oxidative stress, and endothelial dysfunction and the 20-year cumulative incidence of early age-related macular degeneration: the beaver dam eye study. JAMA Ophthalmol. 132, 446–455. 10.1001/jamaophthalmol.2013.7671. [PubMed: 24481424]

Landowski M, Kelly U, Klingeborn M, Groelle M, Ding J-D, Grigsby D, and Bowes Rickman C (2019). Human complement factor H Y402H polymorphism causes an age-related macular degeneration phenotype and lipoprotein dysregulation in mice. Proc. Natl. Acad. Sci. U S A 116, 3703–3711. 10.1073/pnas.1814014116. [PubMed: 30808757]

Lane DJR, Robinson SR, Czerwinska H, Bishop GM, and Lawen A (2010). Two routes of iron accumulation in astrocytes: ascorbate-dependent ferrous iron uptake via the divalent metal transporter (DMT1) plus an independent route for ferric iron. Biochem. J 432, 123–132. 10.1042/bj20101317. [PubMed: 20819077]

Leruez S, Amati-Bonneau P, Verny C, Reynier P, Procaccio V, Bonneau D, and Milea D (2014). Mitochondrial dysfunction affecting visual pathways. Rev. Neurol 170, 344–354. 10.1016/j.neurol.2014.03.009. [PubMed: 24798923]

Li Y, Song D, Song Y, Zhao L, Wolkow N, Tobias JW, Song W, and Dunaief JL (2015). Iron-induced Local Complement Component 3 (C3) Upregulation via Non-canonical Transforming Growth Factor (TGF)-β Signaling in the Retinal Pigment Epithelium. J Biol Chem 290, 11918–11934. 10.1074/jbc.m115.645903. [PubMed: 25802332]

Liuzzi JP, Aydemir F, Nam H, Knutson MD, and Cousins RJ (2006). Zip 14 (Slc39a14) mediates non-transferrin-bound iron uptake into cells. Proc. Natl. Acad. Sci. U S A 103, 13612–13617. 10.1073/pnas.0606424103. [PubMed: 16950869]

Lopez CA, and Skaar EP (2018). The impact of dietary transition metals on host-bacterial interactions. Cell Host Microbe 23, 737–748. 10.1016/j.chom.2018.05.008. [PubMed: 29902439]

Lumeng CN, and Saltiel AR (2011). Inflammatory links between obesity and metabolic disease. J. Clin. Invest 121, 2111–2117. 10.1172/jci57132. [PubMed: 21633179]

Lyssenko NN, Haider N, Picataggi A, Cipollari E, Jiao W, Phillips MC, Rader DJ, and Chavali VRM (2018). Directional ABCA1-mediated cholesterol efflux and apoB-lipoprotein secretion in the retinal pigment epithelium. J. Lipid Res 59, 1927–1939. 10.1194/jlr.m087361. [PubMed: 30076206]

Lyu Y, Zauhar R, Dana N, Strang CE, Hu J, Wang K, Liu S, Pan N, Gamlin P, Kimble JA, et al. (2021). Implication of specific retinal cell-type involvement and gene expression changes in AMD progression using integrative analysis of single-cell and bulk RNA-seq profiling. Sci. Rep 11, 15612. 10.1038/s41598-021-95122-3. [PubMed: 34341398]

Mares-Perlman JA, Brady WE, Klein R, VandenLangenberg GM, Klein BEK, and Palta M (1995). Dietary fat and age-related maculopathy. Arch. Ophthalmol 113,743–748. 10.1001/archopht.1995.01100060069034. [PubMed: 7786215]

McCord JM, and Day ED (1978). Superoxide-dependent production of hydroxyl radical catalyzed by iron-EDTA complex. FEBS Lett. 86, 139–142. 10.1016/0014-5793(78)80116-1. [PubMed: 202505]

McCord JM (1974). Free radicals and inflammation: protection of synovial fluid by superoxide dismutase. Science 185, 529–531. 10.1126/science.185.4150.529. [PubMed: 4841157]

Monteleone M, Stanley AC, Chen KW, Brown DL, Bezbradica JS, von Pein JB, Holley CL, Boucher D, Shakespear MR, Kapetanovic R, et al. (2018). Interleukin-1β maturation triggers its relocation to the plasma membrane for gasdermin-D-dependent and -independent secretion. Cell Rep. 24, 1425–1433. 10.1016/j.celrep.2018.07.027. [PubMed: 30089254]

Nassar K, Grisanti S, Elfar E, Lüke J, Lüke M, and Grisanti S (2015). Serum cytokines as biomarkers for age-related macular degeneration. Graefe's Arch. Clin. Exp. Ophthalmol 253, 699–704. 10.1007/s00417-014-2738-8. [PubMed: 25056526]

Natoli R, Fernando N, Madigan M, Chu-Tan JA, Valter K, Provis J, and Rutar M (2017). Microglia-derived IL-1β promotes chemokine expression by Müller cells and RPE in focal retinal degeneration. Mol. Neurodegener 12, 31. 10.1186/s13024-017-0175-y. [PubMed: 28438165]

Nnah IC, Lee C-H, and Wessling-Resnick M (2020). Iron potentiates microglial interleukin-1β secretion induced by amyloid-β. J. Neurochem 154, 177–189. 10.1111/jnc.14906. [PubMed: 31693761]

Nussenblatt RB, Lee RWJ, Chew E, Wei L, Liu B, Sen HN, Dick AD, and Ferris FL (2014). Immune responses in age-related macular degeneration and a possible long-term therapeutic strategy for prevention. Am. J. Ophthalmol 158, 5–11.e2. 10.1016/j.ajo.2014.03.014. [PubMed: 24709810]

Oh H, Takagi H, Takagi C, Suzuma K, Otani A, Ishida K, Matsumura M, Ogura Y, and Honda Y (1999). The potential angiogenic role of macrophages in the formation of choroidal neovascular membranes. Invest. Ophthalmol. Vis. Sci 40, 1891–1898. [PubMed: 10440240]

Rein DB, Wittenborn JS, Zhang X, Honeycutt AA, Lesesne SB, Saaddine J, and Vision Health Cost-Effectiveness Study Group. (2009). Forecasting age-related macular degeneration through the year 2050: the potential impact of new treatments. Arch. Ophthalmol 127, 533–540. 10.1001/archophthalmol.2009.58. [PubMed: 19365036]

Roddy GW, Rosa RH, Viker KB, Holman BH, Hann CR, Krishnan A, Gores GJ, Bakri SJ, and Fautsch MP (2019). Diet mimicking "fast food" causes structural changes to the retina relevant to age-related macular degeneration. Curr. Eye Res 45, 726–732. 10.1080/02713683.2019.1694156. [PubMed: 31735070]

Seddon JM, Rosner B, Sperduto RD, Yannuzzi L, Haller JA, Blair NP, and Willett W (2001). Dietary fat and risk for advanced age-related macular degeneration. Arch. Ophthalmol 119, 1191–1199. 10.1001/archopht.119.8.1191. [PubMed: 11483088]

Seddon JM, Cote J, and Rosner B (2003a). Progression of age-related macular degeneration: association with dietary fat, transunsaturated fat, nuts, and fish intake. Arch. Ophthalmol 121, 1728–1737. 10.1001/archopht.121.12.1728. [PubMed: 14662593]

Seddon JM, Cote J, Davis N, and Rosner B (2003b). Progression of age-related macular degeneration: association with body mass index, waist circumference, and waist-hip ratio. Arch. Ophthalmol 121, 785–792. 10.1001/archopht.121.6.785. [PubMed: 12796248]

Shanmugam NKN, Chen K, and Cherayil BJ (2015). Commensal bacteria-induced interleukin 1β (IL-1β) secreted by macrophages up-regulates hepcidin expression in hepatocytes by activating the bone morphogenetic protein signaling pathway. J. Biol. Chem 290, 30637–30647. 10.1074/jbc.m115.689190. [PubMed: 26515063]

Silva I, Peccerella T, Mueller S, and Rausch V (2019). IL-1 beta-mediated macrophage-hepatocyte crosstalk upregulates hepcidin under physiological low oxygen levels. Redox Biol. 24, 101209. 10.1016/j.redox.2019.101209. [PubMed: 31108461]

Soares MP, and Hamza I (2016). Macrophages and iron metabolism. Immunity 44, 492–504. 10.1016/j.immuni.2016.02.016. [PubMed: 26982356]

Soares MP, and Weiss G (2015). The Iron age of host–microbe interactions. EMBO Rep. 16, 1482–1500. 10.15252/embr.201540558. [PubMed: 26474900]

Song D, Kanu LN, Li Y, Kelly KL, Bhuyan RK, Aleman T, Morgan JIW, and Dunaief JL (2016). AMD-like retinopathy associated with intravenous iron. Exp Eye Res 151, 122–133. 10.1016/j.exer.2016.08.008. [PubMed: 27565570]

Song D, Song Y, Hadziahmetovic M, Zhong Y, and Dunaief JL (2012). Systemic administration of the iron chelator deferiprone protects against light-induced photoreceptor degeneration in the mouse retina. Free Radic. Biol. Med 53, 64–71. 10.1016/j.freeradbiomed.2012.04.020. [PubMed: 22579919]

Sterling JK, Adetunji MO, Guttha S, Bargoud AR, Uyhazi KE, Ross AG, Dunaief JL, and Cui QN (2020). GLP-1 receptor agonist NLY01 reduces retinal inflammation and neuron death secondary to ocular hypertension. Cell Rep. 33, 108271. 10.1016/j.celrep.2020.108271. [PubMed: 33147455]

Sterling JK, Kam T-I, Guttha S, Park H, Baumann B, Mehrabani-Tabari AA, Schultz H, Anderson B, Alnemri A, Chou S-C, et al. (2022). Interleukin-6 triggers toxic neuronal iron sequestration in response to pathological α-synuclein. Cell Reports 38, 110358–110358. 10.1016/j.celrep.2022.110358. [PubMed: 35172141]

Tarallo V, Hirano Y, Gelfand BD, Dridi S, Kerur N, Kim Y, Cho WG, Kaneko H, Fowler BJ, Bogdanovich S, et al. (2012). DICER1 loss and alu RNA induce age-related macular degeneration via the NLRP3 inflammasome and MyD88. Cell 149, 847–859. 10.1016/j.cell.2012.03.036. [PubMed: 22541070]

Toomey CB, Kelly U, Saban DR, and Bowes Rickman C (2015). Regulation of age-related macular degeneration-like pathology by complement factor H.Proc. Natl. Acad. Sci. USA 112, E3040–E3049. 10.1073/pnas.1424391112. [PubMed: 25991857]

Tseng WA, Thein T, Kinnunen K, Lashkari K, Gregory MS, D'Amore PA, and Ksander BR (2013). NLRP3 inflammasome activation in retinal pigment epithelial cells by lysosomal destabilization: implications for age-related macular degeneration. Invest. Ophthalmol. Vis. Sci 54, 110–120. 10.1167/iovs.12-10655. [PubMed: 23221073]

Tuzcu M, Orhan C, Muz OE, Sahin N, Juturu V, and Sahin K (2017). Lutein and zeaxanthin isomers modulates lipid metabolism and the inflammatory state of retina in obesity-induced high-fat diet rodent model. BMC Ophthalmol 17, 129. 10.1186/s12886-017-0524-1. [PubMed: 28738845]

Vandanmagsar B, Youm Y-H, Ravussin A, Galgani JE, Stadler K, Mynatt RL, Ravussin E, Stephens JM, and Dixit VD (2011). The NLRP3 inflammasome instigates obesity-induced inflammation and insulin resistance. Nat.Med 17, 179–188. 10.1038/nm.2279. [PubMed: 21217695]

Voigt AP, Mulfaul K, Mullin NK, Flamme-Wiese MJ, Giacalone JC, Stone EM, Tucker BA, Scheetz TE, and Mullins RF (2019). Single-cell transcriptomics of the human retinal pigment epithelium and choroid in health and macular degeneration. Proc. Natl. Acad. Sci. U S A 116, 24100–24107. 10.1073/pnas.1914143116. [PubMed: 31712411]

Voigt AP, Whitmore SS, Mulfaul K, Chirco KR, Giacalone JC, Flamme-Wiese MJ, Stockman A, Stone EM, Tucker BA, Scheetz TE, and Mullins RF (2020a). Bulk and single-cell gene expression analyses reveal aging human choriocapillaris has pro-inflammatory phenotype. Microvasc. Res 131, 104031. 10.1016/j.mvr.2020.104031. [PubMed: 32531351]

Voigt AP, Whitmore SS, Lessing ND, DeLuca AP, Tucker BA, Stone EM, Mullins RF, and Scheetz TE (2020b). Spectacle: an interactive resource for ocular single-cell RNA sequencing data analysis. Exp. Eye Res 200, 108204. 10.1016/j.exer.2020.108204. [PubMed: 32910939]

Weber A, Wasiliew P, and Kracht M (2010). Interleukin-1 (IL-1) pathway. Sci. Signal 3, cm1. 10.1126/scisignal.3105cm1. [PubMed: 20086235]

Weiss G, Ganz T, and Goodnough LT (2019). Anemia of inflammation. Blood 133, 40–50. 10.1182/blood-2018-06-856500. [PubMed: 30401705]

Wood H (2020). Brain iron correlates with cognitive change in Parkinson disease. Nat. Rev. Neurol 16, 184. 10.1038/s41582-020-0339-1.

Wu H, and Ballantyne CM (2020). Metabolic inflammation and insulin resistance in obesity. Circ. Res 126, 1549–1564. 10.1161/circresaha.119.315896. [PubMed: 32437299]

Wu J, Peachey NS, and Marmorstein AD (2004). Light-evoked responses of the mouse retinal pigment epithelium. J. Neurophysiol 91, 1134–1142. 10.1152/jn.00958.2003. [PubMed: 14614107]

Wysokinski D, Blasiak J, Dorecka M, Kowalska M, Robaszkiewicz J, Pawlowska E, Szaflik J, and Szaflik JP (2014). Variability of the transferrin receptor 2 gene in AMD. Dis Markers 2014, 507356. 10.1155/2014/507356. [PubMed: 24648608]

Wysokinski D, Danisz K, Blasiak J, Dorecka M, Romaniuk D, Szaflik J, and Szaflik JP (2012). An association of transferrin gene polymorphism and serum transferrin levels with age-related macular degeneration. Exp Eye Res 106, 14–23. 10.1016/j.exer.2012.10.003. [PubMed: 23089144]

Wysokinski D, Danisz K, Pawlowska E, Dorecka M, Romaniuk D, Robaszkiewicz J, Szaflik M, Szaflik J, Blasiak J, and Szaflik JP (2015). Transferrin receptor levels and polymorphism of its gene in age-related macular degeneration. Acta Biochim Pol 62, 177–184. 10.18388/abp.2014_843. [PubMed: 25915522]

Wysokinski D, Szaflik J, Sklodowska A, Kolodziejska U, Dorecka M, Romaniuk D, Wozniak K, Blasiak J, and Szaflik JP (2011). The A Allele of the -576G>A Polymorphism of the Transferrin Gene Is Associated with the Increased Risk of Age-Related Macular Degeneration in Smokers. Tohoku J Exp Medicine 223, 253–261. 10.1620/tjem.223.253.

Zhang M, Chu Y, Mowery J, Konkel B, Galli S, Theos AC, and Golestaneh N (2018). Pgc-1α repression and high-fat diet induce age-related macular degeneration-like phenotypes in mice. Dis. Model. Mech 11, dmm032698. 10.1242/dmm.032698. [PubMed: 29925537]

Zhao M, Bai Y, Xie W, Shi X, Li F, Yang F, Sun Y, Huang L, and Li X (2015). Interleukin-1β level is increased in vitreous of patients with neovascular age-related macular degeneration (nAMD) and polypoidal choroidal vasculopathy (PCV). PLoS One 10, e0125150. 10.1371/journal.pone.0125150. [PubMed: 25978536]

Highlights

- High-fat diet activates the CISR through adipose-derived IL-1β
- Iron chelation protects against obesity-induced RPE dysfunction
- Hallmarks of the CISR are present in AMD patients

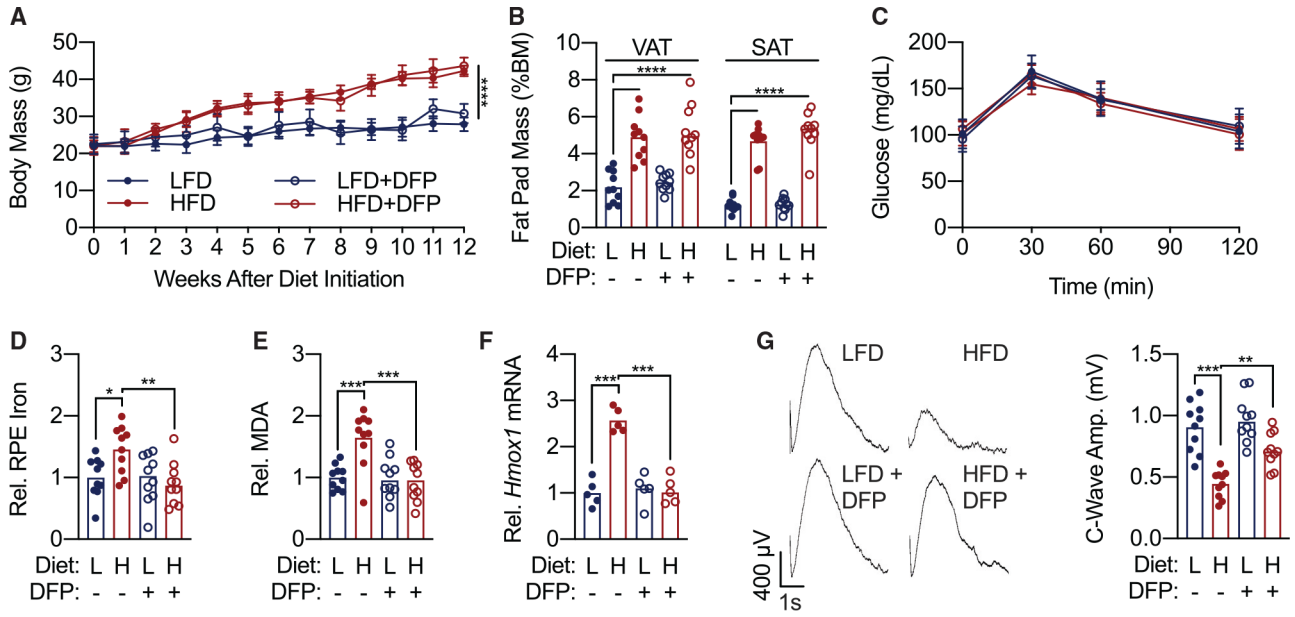

Figure 1. High-fat diet induces iron-dependent RPE dysfunction

(A) Mass in grams of mice fed a low-fat diet (LFD) or high-fat diet (HFD) alone or in combination with iron chelator deferiprone (DFP) (n = 20/group).

(B) Visceral adipose tissue (VAT) and subcutaneous adipose tissue (SAT) hypertrophy were dependent on diet but not DFP treatment (n = 10/group).

(C) Diet and DFP treatment had no effect on glycemic control measured with intraperitoneal glucose tolerance test (n = 10/group).

(D) HFD mice accumulate RPE iron, measured using inductively coupled plasma mass spectrometry, which can be prevented with DFP treatment (n = 10/group).

(E) HFD mice accumulate lipid oxidation product MDA in RPE, which is rescued by treatment with DFP (n = 10/group).

(F) HFD mice RPE upregulate *Hmox1*, measured by qPCR, in an iron-dependent manner (n = 5/group).

(G) HFD mice exhibit c-wave amplitude deficits, measured by electroretinography, which can be partially rescued by iron chelation with DFP (n = 10/group).

Data indicate mean and, where error bars are shown, ± SD. *p < 0.05, **p < 0.01, ***p < 0.001, ****p < 0.0001, by 2-way repeated-measures ANOVA (A and C) or 2-way ANOVA (B and D–G) with Tukey's honestly significant difference (HSD) post hoc test.

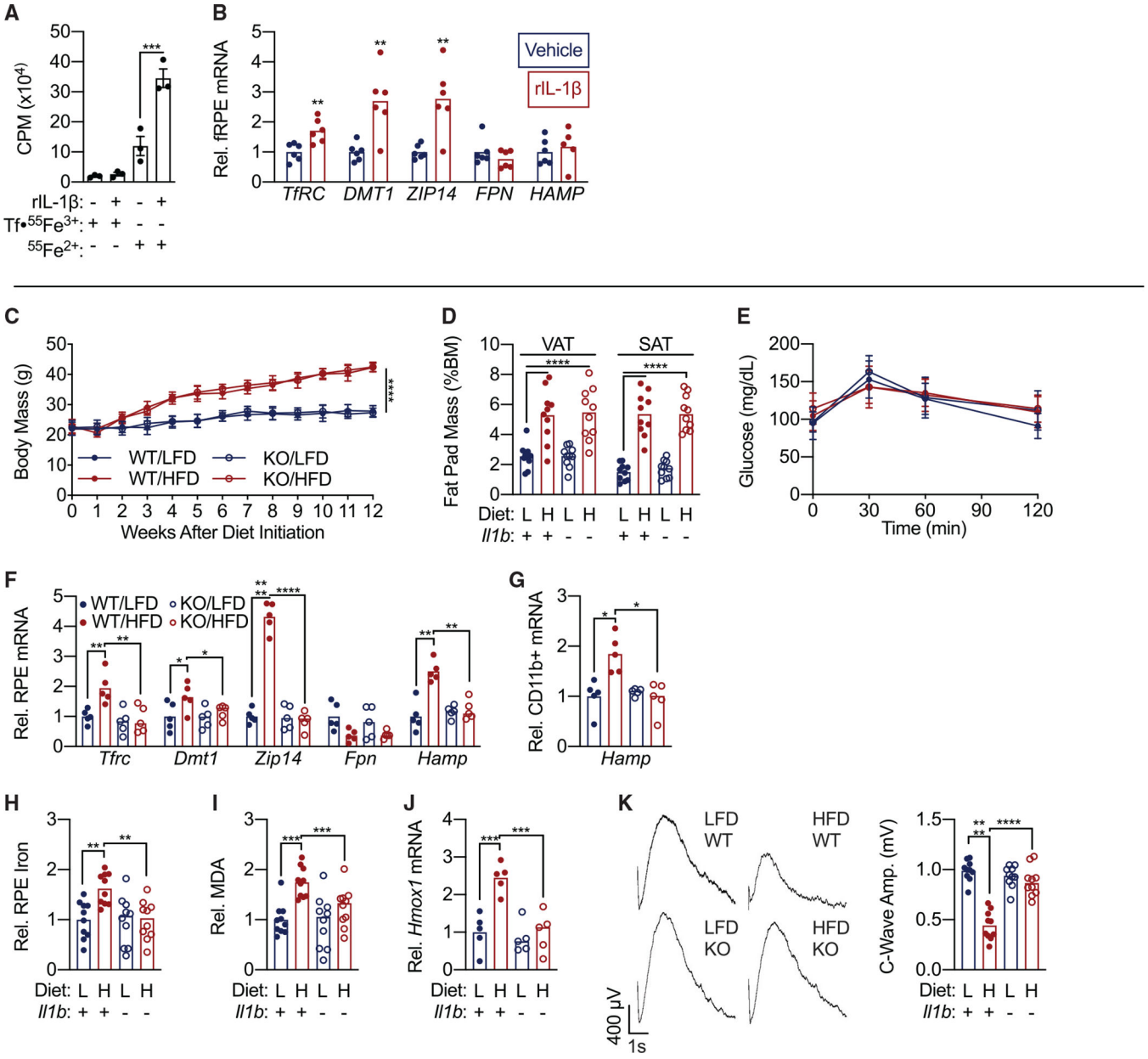

Figure 2. IL-1β is necessary for HFD-induced RPE iron accumulation and dysfunction

(A) Human fetal RPE (fRPE) cultures were treated with either transferrin-bound ferric iron ($Tf{\cdot}^{55}Fe^{3+}$) or ferrous iron ascorbate ($^{55}Fe^{2+}$) alone or in the presence of recombinant IL-1β (rIL-1β). Intracellular iron accumulation in fRPE lysates was measured during 8 h of treatment using a scintillation counter to quantify counts per minute (CPM) (n = 3/group).

(B) fRPE cultures were treated with either media (vehicle) or recombinant IL-1β (rIL-1β) for 8 h before cells were harvested for qPCR analysis of iron transport/ regulatory genes (n = 6/group).

(C) Mass in grams of WT and *Il1b*$^{-/-}$ (KO) mice fed an LFD or an HFD (n = 20/group).

(D) VAT and SAT hypertrophy were dependent on diet but not genotype (n = 10/group).

(E) Diet and genotype had no effect on glycemic control measured with intraperitoneal glucose tolerance test (n = 10/group).
(F) RPE gene expression measured by qPCR following 12 weeks of either LFD or HFD (n = 5/group).
(G) Retinal $CD11b^{+}$ cell gene expression following 12 weeks of either LFD or HFD (n = 5/group).
(H) HFD WT mice accumulate RPE iron, measured using inductively coupled plasma mass spectrometry, which is rescued in the HFD *Il1b*$^{-/-}$ mice (n = 10/group).
(I) HFD WT mice accumulate lipid oxidation product MDA in RPE, which is rescued in HFD *Il1b*$^{-/-}$ mice (n = 10/group).
(J) HFD WT mice RPE upregulate *Hmox1* in an *Il1b*-dependent manner (n = 5/group).
(K) HFD WT mice exhibit c-wave amplitude deficits, measured by electroretinography, which is rescued in HFD *Il1b*$^{-/-}$ mice (n = 10/group).
Data indicate mean and, where error bars are shown, ± SD. *p < 0.05, **p < 0.01, ***p < 0.001, ****p < 0.0001, by 1-way ANOVA with multiple comparisons (A), unpaired Student's t test (B), or 2-way repeated-measures ANOVA (C and E) or 2-way ANOVA (D and F–K) with Tukey's HSD post hoc test.

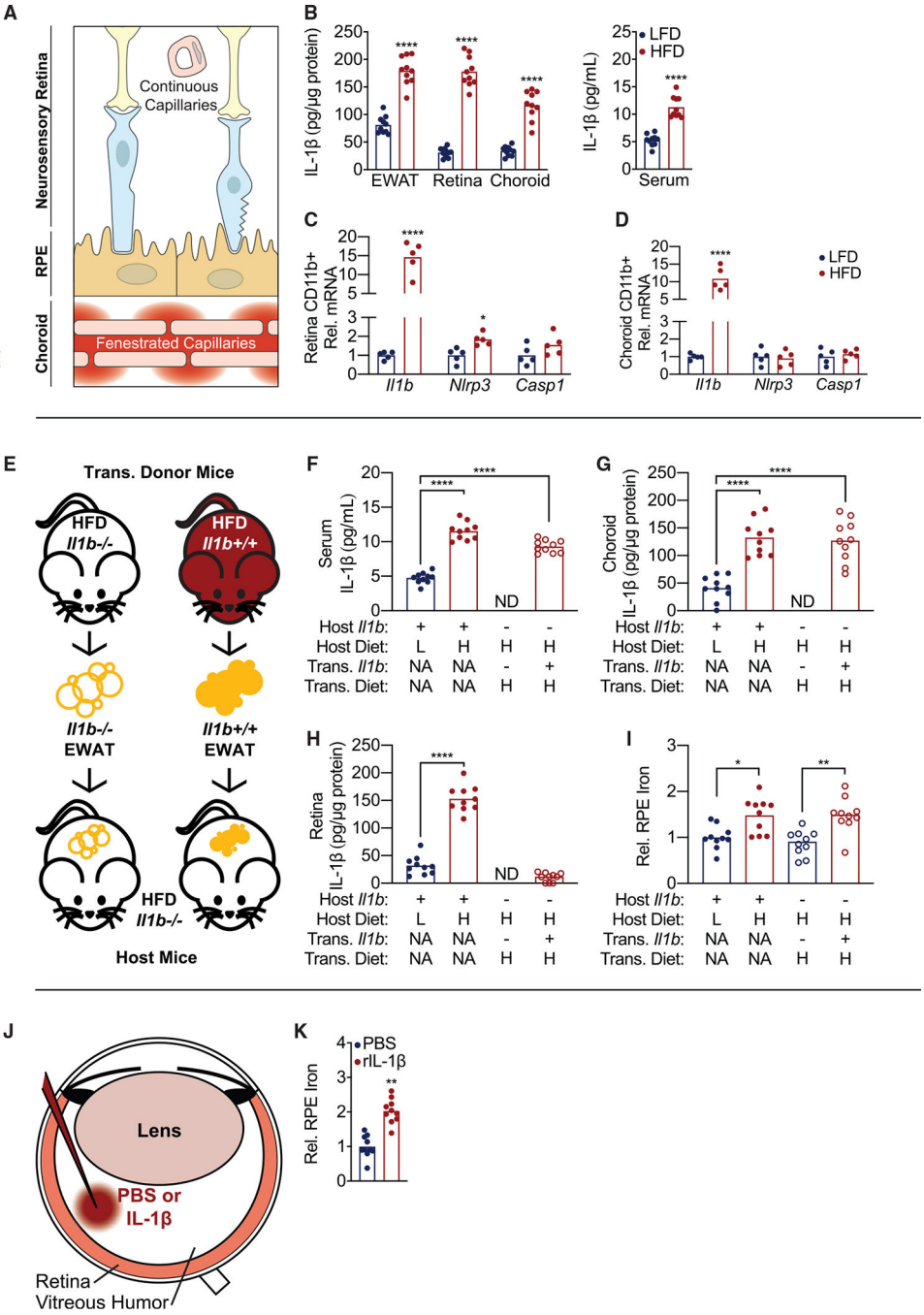

Figure 3. Activation of systemic and local inflammatory circuits contributes to IL-1β production

(A) Schematic of RPE exposed apically to the neurosensory retina behind the blood-retina barrier, and basolaterally to the fenestrated choriocapillaris.

(B) IL-1β ELISA performed on epididymal white adipose tissue (eWAT), retina, choroid, and serum harvested from WT mice fed an LFD or an HFD diet for 12 weeks (n = 10/group).

(C and D) qPCR analysis of *Il1b*, *Nlrp3*, and *Casp1* gene expression in retinal (C) and choroidal (D) $CD11b^{+}$ cells (n = 5/group).

(E) Schematic of eWAT transplant.

(F–H) IL-1β ELISA performed on serum (F), choroid (G), or retina (H) from WT mice fed an LFD or an HFD that underwent a sham transplant surgery (indicated by NA for transplant *Il1b* genotype and diet) or $Il1b^{-/-}$ mice fed an HFD that received eWAT donor tissue from HFD-fed WT or $Il1b^{-/-}$ mice (n = 10/group).

(I) Inductively coupled plasma mass spectrometry (iCP-MS) performed on RPE isolated from WT mice fed an LFD or an HFD that underwent a sham transplant surgery (indicated by NA for transplant *Il1b* genotype and diet) or $Il1b^{-/-}$ mice fed an HFD that received eWAT donor tissue from HFD-fed WT or $Il1b^{-/-}$ mice (n = 10/ group).

(J) Schematic of intravitreal injection.

(K) WT mice received an intravitreal injection of PBS or recombinant IL-1β (rIL-1β). Eight hours after injection, RPE was harvested, and intracellular iron was quantified using iCP-MS (n = 10/group).

Data indicate mean. *p < 0.05, **p < 0.01, and ****p < 0.0001 by unpaired student's t test (B–D and K) or 2-way ANOVA (F–I) with Tukey's HSD post hoc test.

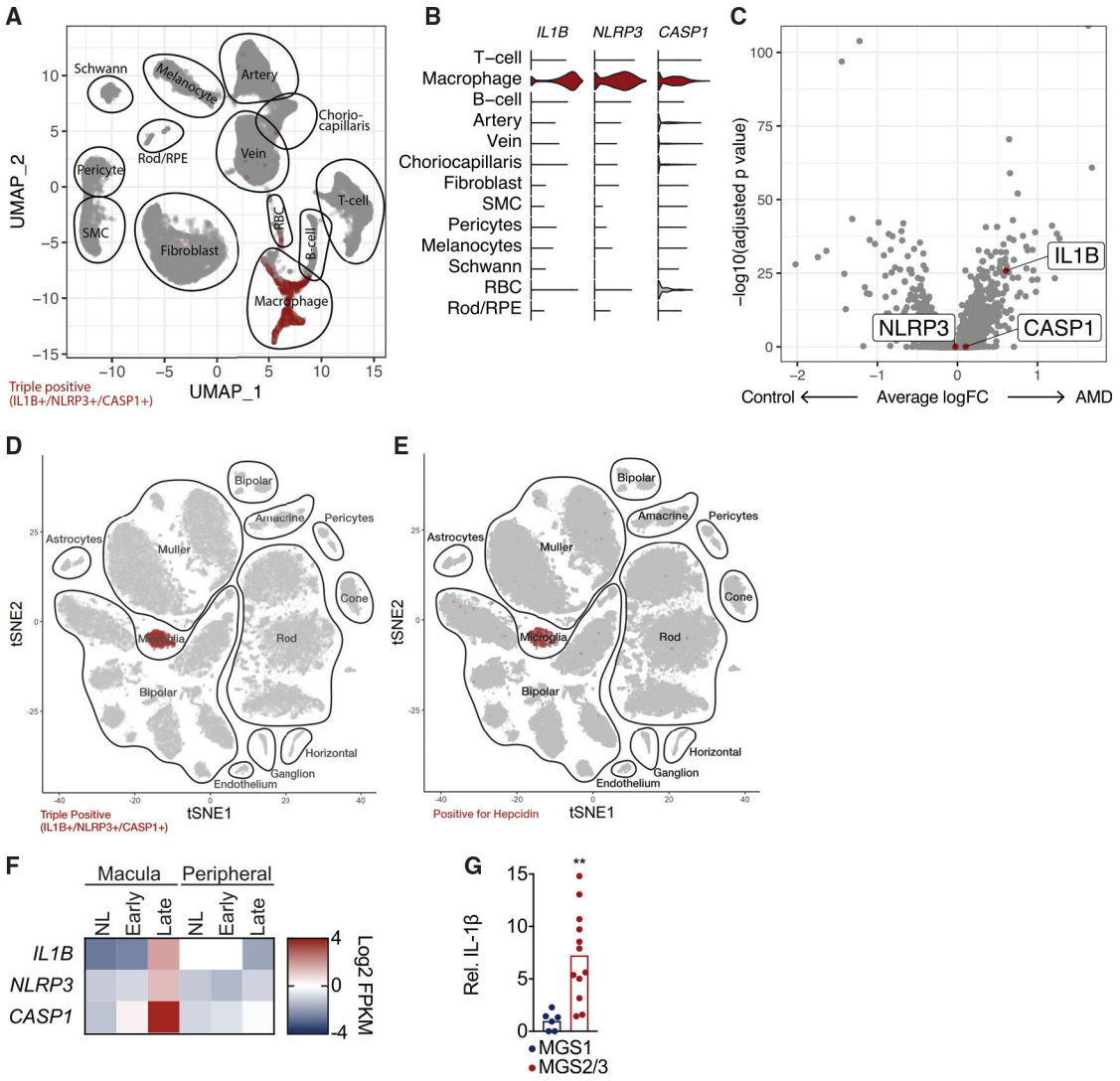

Figure 4. Hallmarks of IL-1β-dependent CISR are observed in AMD patients

(A) Human choroidal single-cell RNA sequencing data. Cells expressing at least one read of *IL1B*, *NLRP3*, and *CASP1* (i.e., triple-positive cells) are colored in red, while the remaining cells are colored in gray. A total of 58.6% of macrophages expressed *IL1B*, *NLRP3*, and *CASP1*.

(B) Violin plots of *IL1B*, *NLRP3*, and *CASP1* expression by cell type indicate macrophage-specific expression of these transcripts.

(C) Using the same single-cell RNA sequencing data, differential expression analysis was performed between macrophages originating from AMD donors(n = 2) versus control donors (n = 4). Differential expression results are displayed in a volcano plot, where positive log fold changes indicate enrichment in AMD samples. Results for *IL1B*, *CASP1*, and *NLRP3* are highlighted.

(D) Visualization of healthy human neurosensory retina single-cell clusters using t-distributed stochastic neighbor embedding (t-SNE) sequencing data from normal retinas. Cells expressing at least one read of *IL1B*, *NLRP3*, and *CASP1* (i.e., triple-positive cells)

are colored in red, while the remaining cells are colored in gray. Enrichment in these three transcripts is specific to microglia.

(E) Visualization of healthy human neurosensory retina single-cell clusters using t-SNE sequencing data from normal retinas. Cells expressing at least one read of *HAMP* (protein name hepcidin) are colored in red, while the remaining cells are colored in gray. Enrichment in *HAMP* is specific to microglia.

(F) Bulk neurosensory retina RNA sequencing on normal (NL), early AMD, and late AMD macular retina or peripheral retina showing expression of *IL1B*, *NLRP3*, and *CASP1* across disease progression in a region-specific manner. Color scale corresponds to log2 of expression measured in fragments per kilobase of transcript per million mapped reads (FPKM).

(G) IL-1β ELISA performed on neurosensory retina from eyes without AMD (MGS1, n = 6) and with early (MGS2, n = 6) or intermediate (MGS3, n = 6) AMD. See Table S1 for donor information.

**$p < 0.01$ by unpaired Student's t test (J).

KEY RESOURCES TABLE

REAGENT or RESOURCE	SOURCE	IDENTIFIER
Antibodies		
anti-Astrocyte cell surface antigen 2 (ACSA-2)	Miltenyi Biotec	130-097-678; RRID:AB_2894998
anti-CD11b	Miltenyi Biotec	130-126-725
Chemicals, peptides, and recombinant proteins		
Deferiprone	ApoPharma	N/A
Recombinant human IL-1β protein	Abcam	ab9617
Recombinant mouse IL-1β protein	LSBio	LS-G51411
Critical commercial assays		
MDA ELISA	Abcam	ab238537
Mouse IL-1β ELISA	R&D Systems	MLB00C
Human IL-1β ELISA	R&D Systems	DLB50
Deposited data		
Human choroidal scRNA-seq data	Voigt et al. (2019)	GSE135922 donors 4–7 (control), 22–23 (AMD)
Neurosensory retina scRNA-seq data	Lyu et al. (2021)	GSE155288
Neurosensory retina bulk RNA-seq data	Lyu et al. (2021)	GSE155154
Experimental models: Organisms/strains		
C57BL6/J Wild-Type	Jackson Labs	000664
IL-1β Knockout	Dr. Iwakura, University of Tokyo	N/A
Experimental models: Cell culture		
Fetal RPE Cell Cultures	Advanced Bioscience Resources Inc.	N/A
Software and algorithms		
Seurat R package	Butler et al. (2018)	https://satijalab.org/seurat/
Other		

REAGENT or RESOURCE	SOURCE	IDENTIFIER
Rodent diet with 10% fat (low fat diet)	Research Diets	D12450
Rodent diet with 60% fat (high fat diet)	Research Diets	D12492